Title

High-resolution imaging and quantification of plasma membrane cholesterol by NanoSIMS

Journal

Proceedings of the National Academy of Sciences of the United States of America, 114(8)

ISSN

0027-8424

Authors

He, Cuiwen
Hu, Xuchen
Jung, Rachel S
et al.

Publication Date

2017-02-21

DOI

10.1073/pnas.1621432114

Peer reviewed

High-resolution imaging and quantification of plasma membrane cholesterol by NanoSIMS

Cuiwen He[a], Xuchen Hu[a], Rachel S. Jung[a], Thomas A. Weston[a], Norma P. Sandoval[a], Peter Tontonoz[b,c], Matthew R. Kilburn[d], Loren G. Fong[a], Stephen G. Young[a,e,1,2], and Haibo Jiang[d,1,2]

[a]Department of Medicine, University of California, Los Angeles, CA 90095; [b]Department of Pathology and Laboratory Medicine, University of California, Los Angeles, CA 90095; [c]Howard Hughes Medical Institute, University of California, Los Angeles, CA 90095; [d]Centre for Microscopy, Characterisation and Analysis, University of Western Australia, Perth 6009, Australia; and [e]Department of Human Genetics, University of California, Los Angeles, CA 90095

Contributed by Stephen G. Young, January 3, 2017 (sent for review December 21, 2016; reviewed by Yunbin Guan, Fredric B. Kraemer, Sampath Parthasarathy, and Joseph L. Witztum)

Cholesterol is a crucial lipid within the plasma membrane of mammalian cells. Recent biochemical studies showed that one pool of cholesterol in the plasma membrane is "accessible" to binding by a modified version of the cytolysin perfringolysin O (PFO*), whereas another pool is sequestered by sphingomyelin and cannot be bound by PFO* unless the sphingomyelin is destroyed with sphingomyelinase (SMase). Thus far, it has been unclear whether PFO* and related cholesterol-binding proteins bind uniformly to the plasma membrane or bind preferentially to specific domains or morphologic features on the plasma membrane. Here, we used nanoscale secondary ion mass spectrometry (NanoSIMS) imaging, in combination with ^{15}N-labeled cholesterol-binding proteins (PFO* and ALO-D4, a modified anthrolysin O), to generate high-resolution images of cholesterol distribution in the plasma membrane of Chinese hamster ovary (CHO) cells. The NanoSIMS images revealed preferential binding of PFO* and ALO-D4 to microvilli on the plasma membrane; lower amounts of binding were detectable in regions of the plasma membrane lacking microvilli. The binding of ALO-D4 to the plasma membrane was virtually eliminated when cholesterol stores were depleted with methyl-β-cyclodextrin. When cells were treated with SMase, the binding of ALO-D4 to cells increased, largely due to increased binding to microvilli. Remarkably, lysenin (a sphingomyelin-binding protein) also bound preferentially to microvilli. Thus, high-resolution images of lipid-binding proteins on CHO cells can be acquired with NanoSIMS imaging. These images demonstrate that accessible cholesterol, as judged by PFO* or ALO-D4 binding, is not evenly distributed over the entire plasma membrane but instead is highly enriched on microvilli.

NanoSIMS | cholesterol | microvilli | anthrolysin O | perfringolysin O

In recent biochemical studies, Das et al. analyzed the binding of PFO*, a mutant version of the cytolysin perfringolysin O, to cholesterol in the plasma membrane of several mammalian cells, including human fibroblasts and Chinese hamster ovary (CHO) cells (1, 2). They found that plasma membrane cholesterol is "accessible" to ^{125}I-PFO* binding when cholesterol levels are high (exceeding 35 mol% of all membrane lipids). When cholesterol stores were depleted with 2-hydroxypropyl-β-cyclodextrin, the binding of ^{125}I-PFO* to cells was virtually abolished. Interventions that increased plasma membrane cholesterol levels resulted in more ^{125}I-PFO* binding (1). They went on to show that much of the cholesterol in the plasma membrane is sequestered by sphingomyelin and cannot bind ^{125}I-PFO* unless the sphingomyelin is destroyed with sphingomyelinase (SMase) (2). The studies by Das et al. were very important because they characterized distinct pools of cholesterol in the plasma membrane (an accessible pool and a sphingomyelin-sequestered pool); however, the distribution of PFO* binding sites on the plasma membrane was not addressed.

The plasma membrane of mammalian cells is often assumed to contain microdomains (called "lipid rafts") enriched in sphingomyelin and cholesterol. These microdomains can be purified from the plasma membrane by taking advantage of their resistance to detergent extraction at low temperatures (3). Cholesterol- and sphingolipid-rich microdomains are transient and small (<200 nm), making them very difficult to visualize by confocal microscopy (4). To better define the distributions of cholesterol and sphingolipids in the plasma membrane, Frisz et al. (5) used nanoscale secondary ion mass spectrometry (NanoSIMS) imaging to visualize ^{18}O-labeled cholesterol and ^{15}N-labeled sphingolipids in the plasma membrane of 3T3 fibroblasts. They reported that the cholesterol in the plasma membrane was evenly distributed, whereas sphingolipids were found in large (~2–3 μm) and unevenly distributed patches (5). The distinct distributions of cholesterol and sphingolipids in the plasma membrane were somewhat surprising, given that these lipids are thought to interact within the plasma membrane. Of course, the conclusions regarding the plasma membrane distributions of cholesterol and sphingolipids in this NanoSIMS study relied on the assumption that the ^{18}O and ^{15}N ions originated exclusively from the plasma membrane (rather than being derived in part from internal membrane compartments).

In our current study, we used NanoSIMS imaging along with ^{15}N-labeled cholesterol- and sphingomyelin-binding proteins (cytolysins) to visualize distributions of cholesterol and sphingomyelin in the plasma membrane. We reasoned that NanoSIMS imaging with lipid-binding proteins would hold several advantages.

Significance

Biochemical studies have demonstrated that one pool of cholesterol in the plasma membrane is accessible to binding by bacterial cholesterol-binding proteins, whereas another pool is "sequestered" and inaccessible to binding by those proteins. Here, we used nanoscale secondary ion mass spectrometry (NanoSIMS) imaging, along with cholesterol-binding proteins that had been labeled with a stable isotope, to visualize and quantify the distribution of "accessible cholesterol" on the plasma membrane of mammalian cells. Our studies revealed that accessible cholesterol, as judged by cholesterol-binding proteins, is not evenly distributed on the plasma membrane but instead is enriched on the surface of microvilli. The accessible cholesterol on microvilli could be relevant to the movement of cholesterol away from the plasma membrane.

Author contributions: C.H., L.G.F., S.G.Y., and H.J. designed research; C.H., X.H., R.S.J., T.A.W., N.P.S., M.R.K., and H.J. performed research; C.H., P.T., S.G.Y., and H.J. analyzed data; and S.G.Y. and H.J. wrote the paper.

Reviewers: Y.G., California Institute of Technology; F.B.K., VA Palo Alto Health Care System and Stanford University; S.P., University of Central Florida; and J.L.W., University of California, San Diego.

The authors declare no conflict of interest.

[1]S.G.Y. and H.J. contributed equally to this work.

[2]To whom correspondence may be addressed. Email: sgyoung@mednet.ucla.edu or haibo.jiang@uwa.edu.au.

This article contains supporting information online at www.pnas.org/lookup/suppl/doi:10.1073/pnas.1621432114/-/DCSupplemental.

First, we suspected that the ^{15}N signal would be robust. The cholesterol- and sphingomyelin-binding proteins were uniformly labeled with ^{15}N and therefore contained >100 ^{15}N atoms. In contrast, there is only a single ^{18}O atom in [^{18}O]cholesterol. Second, when lipid-binding cytolysins such as PFO* are incubated with cells, one can be confident that they bind to the plasma membrane and not to internal membrane compartments. Third, NanoSIMS instruments can collect ion images with spatial resolutions that are higher than typically obtained with confocal microscopy (6). Fourth, the NanoSIMS instrument collects millions of ions, making it possible to quantify binding of ^{15}N-labeled proteins to morphologically distinct regions within the plasma membrane. Finally, one can judge the validity of NanoSIMS imaging studies according to the lessons from earlier biochemical studies (e.g., the fact that PFO* binding is reduced by cholesterol depletion and increased by treating cells with SMase).

Materials and Methods

CHO-K1 Cells. Stock cultures of hamster CHO-K1 cells were grown in monolayer cultures at 37 °C with 8–9% (vol/vol) CO_2 and maintained in medium A [Ham's F-12 Nutrient Mixture (Thermo Fisher Scientific) containing 10% (vol/vol) FBS (HyClone), 2 mM glutamine, and antibiotic-antimycotic from Gibco containing 100 units/mL of penicillin, 100 μg/mL of streptomycin, and 0.25 μg/mL of amphotericin B]. Medium B is identical to medium A except that it contains 10% (vol/vol) lipoprotein-deficient serum (LPDS) rather than FBS. Medium C is medium B containing 50 μM mevastatin (Calbiochem) and 50 μM mevalonolactone (Sigma). To produce LPDS, FBS was adjusted to a density of 1.21 g/mL with NaBr and centrifuged in a SW41 rotor at 38,000 rpm for 48 h. The top layer (lipoproteins) was discarded, and the bottom fraction (LPDS) was dialyzed against PBS and sterilized with a 0.22-μm filter. For NanoSIMS analysis, cells were grown on 0.5-cm^2 silicon wafers coated with poly-L-lysine or were plated on Thermanox plastic coverslips (Thermo Fisher Scientific). For immunofluorescence microscopy, CHO-K1 cells were plated on glass coverslips in 24-well plates.

To load CHO-K1 cells with cholesterol, cholesterol was dissolved in ethanol and then added to medium C [final cholesterol concentration, 300 μM; final ethanol concentration, 1.17% (vol/vol)]. The cells were then grown in cholesterol-supplemented medium C for 2 d. After three 10-min washes with Dulbecco's PBS containing Mg^{2+} and Ca^{2+} (DPBS+Mg^{2+}+Ca^{2+}), cells were incubated in medium B without cholesterol for 44 h. Finally, the cells were washed three times for 10 min in DPBS+Mg^{2+}+Ca^{2+} containing 0.2% (wt/vol) BSA. To deplete cholesterol, cells were incubated with 10 mM methyl-β-cyclodextrin (MβCD, Sigma) in Ham's F-12 Nutrient Mixture at 37 °C for 15 min. To release the sphingomyelin-sequestered pool of cholesterol on the plasma membrane, cells were incubated at 37 °C for 30 min in medium A containing 100 milliunits/mL of sphingomyelinase from *Staphylococcus aureus* (Sigma). For a "no treatment" control, cells were simply incubated in medium A at 37 °C for 30 min.

Preparation of ^{15}N-labeled His-Tagged PFO*. PFO* is a 500-amino acid noncytolytic cysteine-less version of perfringolysin O (PFO) carrying a Y181A substitution (1). A plasmid for His-tagged PFO* (1) (from Arun Radhakrishnan, University of Texas Southwestern, Dallas, TX) was expressed in BL21(DE3) pLysS *Escherichia coli* (Invitrogen), and the cells were induced with 0.5 mM IPTG in minimal medium containing 95.5 mM KH_2PO_4, 57.4 mM K_2HPO_4, 63.4 mM Na_2HPO_4, 13.8 mM K_2SO_4, 20.2 mM $^{15}NH_4Cl$ (Cambridge Isotope Laboratories), 5 mM $MgCl_2$, 0.2% (wt/vol) glucose, and 100 μg/mL carbenicillin at 37 °C for 16 h. Cells were pelleted at 8,000 × *g* for 20 min at 4 °C and resuspended in 20 mL of buffer containing 50 mM NaH_2PO_4 (pH 7.0), 300 mM NaCl, 2 mM PMSF, and a protease inhibitor mixture tablet (Roche Complete, Mini, EDTA-free; 1 tablet/10 mL). Cells were disrupted by sonication, pulse 1.5 min on and 30 s off (four times). The lysate was centrifuged at 18,000 × *g* for 40 min at 4 °C, and the supernatant was mixed with 4 mL of HisPur Cobalt resin [50% (vol/vol) slurry, Thermo Fisher Scientific] equilibrated in an equilibration buffer [50 mM NaH_2PO_4 (pH 7.0) and 300 mM NaCl] with 10 mM imidazole for 45 min at 4 °C. The mixture was then loaded into a column and the flow through was allowed to drain by gravity from the resin. The column was washed with four column volumes (CVs) of the equilibration buffer plus 10 mM imidazole and 4 CVs of equilibration buffer containing 50 mM imidazole. [^{15}N]PFO* was eluted with 12 CVs of the equilibration buffer containing 300 mM imidazole. Eluates were pooled and concentrated to 2 mL with an Amicon 10-kDa MWCO concentrator (Millipore). Purified protein was stored in 50% (vol/vol) antibody stabilizer PBS (CANDOR Bioscience) at 4 °C.

Preparation of ^{15}N-Labeled His-Tagged Domain 4 of Anthrolysin O. A plasmid for domain 4 of anthrolysin O (ALO-D4, ALO amino acids 404–512 with C472A and S404C substitutions) was obtained from Arun Radhakrishnan. ALO-D4 was expressed and purified in BL21(DE3) pLysS *E. coli* (7). ^{15}N-labeled ALO-D4 was purified as described for ^{15}N-labeled PFO*.

Preparation of ^{15}N-Labeled His-mCherry-Tagged Lysenin. To express a nontoxic version of lysenin, the sequences for lysenin amino acids 161–297 were cloned into the vector pBADmCherry (Addgene). The cDNA for lysenin was synthesized by Integrated DNA Technologies. The vector pBADmCherry was linearized by PCR with primers 5′-TAAGAATTCGAAGCTTGGCTG-3′ and 5′-CTTGTACAGCTCGTCCATGC-3′, and the lysenin cDNA was inserted with the In-Fusion HD Cloning kit (Clontech). Lysenin was expressed in BL21(DE3) *E. coli* (Invitrogen). To produce [^{15}N]lysenin, *E. coli* were grown in 1 L $^{15}NH_4Cl$ minimum media and induced with 0.2% (wt/vol) arabinose at 20 °C for 16 h. Cells were pelleted at 8,000 × *g* for 20 min at 4 °C and resuspended in 20 mL of lysis buffer containing 20 mM NaH_2PO_4 (pH 8.0), 150 mM NaCl, 1 mg/mL lysozyme, 0.4 mg/mL PMSF, and a protease inhibitor mixture tablet (1 tablet/20 mL, Roche, Complete, Mini, EDTA-free). Cells were disrupted with 15 strokes in a Dounce homogenizer, incubated at 4 °C for 3 h and again subjected to Dounce homogenization and sonication. The lysate was centrifuged at 25,000 × *g* for 1 h at 4 °C. The supernatant was loaded onto a 1-mL nickel-nitrilotriacetic acid (Ni-NTA) column (GE Healthcare) equilibrated in equilibration buffer (20 mM NaH_2PO_4, pH 8.0, 150 mM NaCl). The column was washed with 50 column volumes of equilibration buffer containing 30 mM imidazole; the [^{15}N]lysenin was eluted with equilibration buffer containing a linear gradient of imidazole (30–300 mM). Fractions containing lysenin were pooled and concentrated to 1 mL with an Amicon 10-kDa MWCO concentrator (Millipore). The 1-mL eluate was further purified by gel filtration on a Superdex 200 10/300 column (GE Healthcare). Purified protein was stored in 50% (vol/vol) antibody stabilizer PBS (CANDOR Bioscience) at 4 °C.

[^{15}N]PFO* and [^{15}N]ALO-D4 Binding to Cells. CHO-K1 cells were washed three times (10 min each) with DPBS+Mg^{2+}+Ca^{2+} plus 0.2% BSA to remove MβCD or SMase. Each coverslip or silicon wafer containing CHO-K1 cells was incubated in 24-well plates for 2 h at 4 °C with 0.4 mL of binding buffer (25 mM Hepes-KOH, pH 7.4, 150 mM NaCl, 0.2% BSA) containing 20 μg/mL of [^{15}N]ALO-D4 or 20 μg/mL of [^{15}N]PFO*. The cells were washed three times (3 min each) with ice-cold DPBS+Mg^{2+}+Ca^{2+} to remove unbound [^{15}N]ALO-D4 or [^{15}N]PFO*.

[^{15}N]Lysenin Binding to Cells. Cells grown on silicon wafers were washed three times for 10 min with DPBS+Mg^{2+}+Ca^{2+} plus 0.2% BSA to remove MβCD or SMase. Each wafer was incubated in a 24-well plate for 1 h at 4 °C with 0.4 mL of DPBS+Mg^{2+}+Ca^{2+} containing 0.2% BSA and 20 μg/mL of [^{15}N]lysenin. To remove unbound protein, cells were washed three times for 3 min with ice-cold DPBS+Mg^{2+}+Ca^{2+}.

Preparing Cells on Silicon Wafers for NanoSIMS Imaging and Scanning Electron Microscopy. CHO cells were fixed with 4% (vol/vol) paraformaldehyde (PFA) and 1% glutaraldehyde for 20 min at 4 °C, followed by 2.5% (vol/vol) glutaraldehyde in 0.1 M phosphate buffer for 1 h at room temperature. Cells were then washed three times for 10 min with 0.1 M phosphate buffer followed by two 5-min washes with ddH_2O. The cells were then air dried and used for NanoSIMS imaging. For scanning electron microscopy, cells were coated with 5-nm platinum and transferred to a FEI Verios SEM. Images were taken with a 2-KeV incident beam of 50-pA current at a 2.5-mm working distance. In a separate fixation method, cells were fixed in a solution containing 2.5% (vol/vol) glutaraldehyde in 0.1 M sodium cacodylate for 1 h. The samples were rinsed three times with 0.1 M sodium cacodylate before being postfixed in a solution of 1% osmium tetroxide in 0.1 M sodium cacodylate for 40 min followed by three rinses with H_2O. Next, the cells were dehydrated with a graded series of ethanol concentrations and then by critical point drying (Tousimis Autosamdri 810). The samples on stubs were then coated with gold palladium (Pelco SC-70) and imaged with a Zeiss Supra 40VP scanning electron microscope with a 7-KeV incident beam.

Preparation of Epoxy-Embedded Cells for NanoSIMS Imaging. CHO-K1 cells were plated on Thermanox plastic coverslips in a 24-well plate. Cells were loaded with cholesterol, treated with MβCD or SMase, and incubated with [^{15}N]ALO-D4 as described. Next, the cells were fixed with ice-cold 4% (vol/vol) PFA and 1% glutaraldehyde for 20 min at 4 °C, followed by 2.5% (vol/vol) glutaraldehyde in 0.1 M phosphate buffer for 1 h at room temperature. The cells were washed, then incubated in 1% osmium tetroxide in 0.1 M phosphate buffer for 1 h, and washed again with ddH_2O. The cells were then incubated with 2% (vol/vol) aqueous uranyl acetate overnight

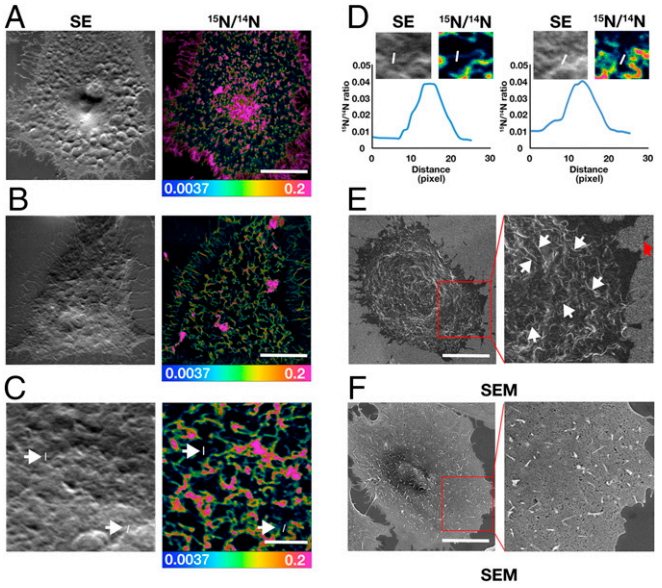

Fig. 1. NanoSIMS imaging of cholesterol-binding proteins on the plasma membrane of CHO-KI cells. CHO-K1 cells were plated on silicon wafers and grown in Ham's F-12 medium containing 10% lipoprotein-deficient serum (*Materials and Methods*) for 5 d. The cells were then loaded with cholesterol as described in *Materials and Methods*. The cells were subsequently grown in medium lacking supplemental cholesterol for 44 h. Next, the cells were incubated with 20 μg/mL [^{15}N]PFO* (*A*) or [^{15}N]ALO-D4 (*B*) for 2 h at 4 °C. NanoSIMS images were generated based on secondary electrons (SEs); other images were created based on the ^{15}N/^{14}N ratio. (Scale bar, 10 μm.) The color scale shows the range of ^{15}N/^{14}N ratios. (*C*) High-magnification image of the cell shown in *B*. (Scale bar, 3 μm.) (*D*) Line scan demonstrating the ^{15}N/^{14}N isotope ratio across microvilli on the surface of the plasma membrane (white lines in *C* and *D*). Pixel, ~19.5 nm. (*E*) SEM image of a CHO-K1 cell grown on a silicon wafer and fixed with 4% (vol/vol) PFA plus 1% glutaraldehyde followed by 2.5% (vol/vol) glutaraldehyde. A higher-magnification image of the boxed area on the *Left* is shown in the image on the *Right*. Red arrow shows a microvillus at the perimeter of the cell; white arrows show microvilli on the surface of the cell. (*F*) SEM image of CHO-K1 cells grown on a silicon wafer and fixed with 2.5% (vol/vol) glutaraldehyde in 0.1 M sodium cacodylate followed by 1% osmium tetroxide in 0.1 M sodium cacodylate. (Scale bar, 10 μm.)

at 4 °C, washed, dehydrated with a graded series of ethanol, transferred to propylene oxide, and infiltrated with a 1:1 mix of propylene oxide:eponate 12 resin (Ted Pella) for 1 h and a 1:2 mix of propylene oxide:resin overnight. The cells were then transferred to fresh resin and embedded by inverting the coverslip onto a Beem capsule filled with fresh resin and polymerized for 24 h at 60 °C. The coverslips were removed and 500-nm thick sections were cut en face with a Diatome diamond knife. The sections were placed on a silicon wafer for NanoSIMS imaging.

Imaging of ALO-D4 and Lysenin Binding with NanoSIMS and Confocal Microscopy. Samples of cells on silicon wafers were coated with 5-nm platinum and transferred to a NanoSIMS 50L instrument (CAMECA) for analysis. An 8-KeV $^{133}Cs^+$ beam was used as the primary ion beam to bombard the sample; secondary ions of −8 KeV ($^{12}C^-$, $^{16}O^-$, $^{12}C^{14}N^-$, $^{12}C^{15}N^-$) and secondary electrons (SEs) were collected. An area of 30 × 30 μm was imaged with a ~1.5-pA beam current (primary aperture D1 = 2) and a dwell time of 10,000 μs/pixel. Scans of 256 × 256 or 512 × 512 pixels were obtained. To obtain high-resolution images, a smaller primary aperture (D1 = 3, ~0.8 pA) was used to image a region of 10 × 10 μm. For embedded sections on silicon wafers, a high primary beam current of ~3.5 nA was used to presputter a 40 × 40 μm region for 2 min to remove the platinum coating and implant $^{133}Cs^+$ for a steady state of secondary ions. In the same region, an area of 30 × 30 μm was then imaged with a ~1.5 pA beam current and a dwell time of 30,000 μs/pixel. Scans of 256 × 256 pixels were obtained. To quantify the ^{15}N/^{14}N ratio, regions of interest were defined and ^{15}N/^{14}N ratios were measured with the OpenMIMS plugin and then processed by Prism 7.0. Regions of interest (including line scans) on images were drawn pixel by pixel for microvilli and nonmicrovilli regions. The mass ratio of ^{15}N/^{14}N was measured with a median filter of 1-pixel radius. The mean and SDs of the ^{15}N/^{14}N ratio data points were then calculated and processed by Prism 7.0. Confocal fluorescence microscopy images were obtained with standard experimental approaches (*SI Materials and Methods*) and recorded with an Axiovert 200 M microscope.

Results

In our first experiments, we used NanoSIMS imaging of [^{15}N]PFO* to visualize the accessible pool of cholesterol on the plasma membrane of CHO-K1 cells. Cells were grown on silicon wafers (1) in cholesterol-rich medium and then incubated with [^{15}N]PFO*. After washing the cells and fixing them with paraformaldehyde, NanoSIMS imaging was performed (Fig. 1*A*). The binding of [^{15}N]PFO* to cells was visualized with images generated from the ratio of $^{12}C^{15}N^-$ and $^{12}C^{14}N^-$ secondary ions (i.e., ^{15}N/^{14}N images). The ^{15}N/^{14}N ratio was high in microvilli extending from the edge of cells and in microvilli fixed to the top surface of cells (Fig. 1*A*). SE images were useful for cell morphology (Fig. 1*A*).

PFO* forms large oligomers when it binds to membranes containing cholesterol (8), and we were concerned that PFO* oligomerization might influence the distribution of [^{15}N]PFO* binding. For that reason, we performed NanoSIMS imaging with another cholesterol-binding protein, ALO-D4, which binds cholesterol in a manner similar to PFO* but does not form large oligomers (7). NanoSIMS images of [^{15}N]ALO-D4 binding to CHO cells were similar to those obtained with [^{15}N]PFO* (Fig. 1*B*); both bound preferentially to microvilli. Preferential binding of [^{15}N]ALO-D4 to microvilli was also evident in high-resolution

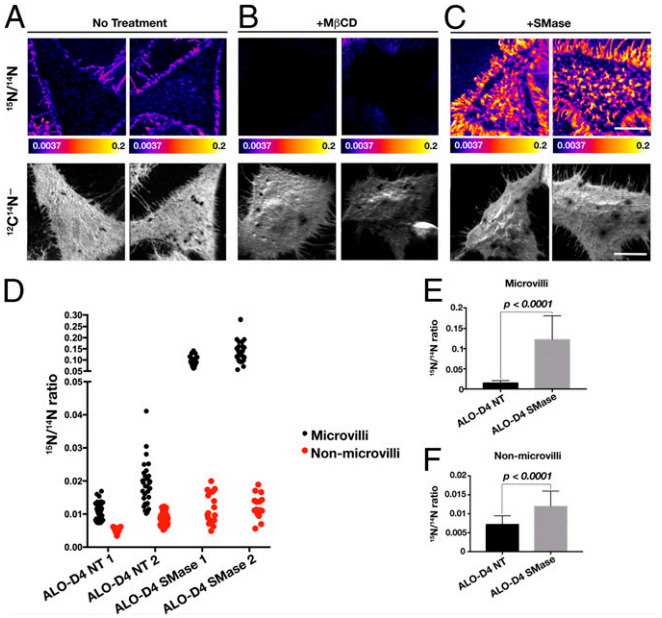

Fig. 2. NanoSIMS analysis of [^{15}N]ALO-D4 binding to the plasma membrane of CHO-KI cells grown under standard conditions. CHO-K1 cells (imaged in *A*–*C*) were plated on silicon wafers and grown overnight and given either no treatment (*A*); treated with 10 mM methyl-β-cyclodextrin (+MβCD) for 15 min at 37 °C (*B*); or treated with 100 milliunits/mL of sphingomyelinase for 30 min at 37 °C (+SMase) (*C*). The cells were then washed and incubated with 20 μg/mL [^{15}N]ALO-D4 for 2 h at 4 °C. NanoSIMS images were generated based on $^{12}C^{14}N^-$ ions (to visualize cell morphology) and on the ^{15}N/^{14}N ratio. (Scale bar, 10 μm.) The color scale shows the range of ^{15}N/^{14}N ratios. (*D*) ^{15}N/^{14}N ratios in microvilli (black solid circles) and nonmicrovilli regions (red solid circles) (n = 30) of the plasma membrane of two nontreated (NT) and SMase-treated (SMase) CHO-K1 cells. (*E* and *F*) Bar graphs depicting ^{15}N/^{14}N ratios in microvilli and nonmicrovilli regions of the plasma membrane in NT and SMase-treated cells. Data were analyzed with an unpaired Student's t test with Welch's correction.

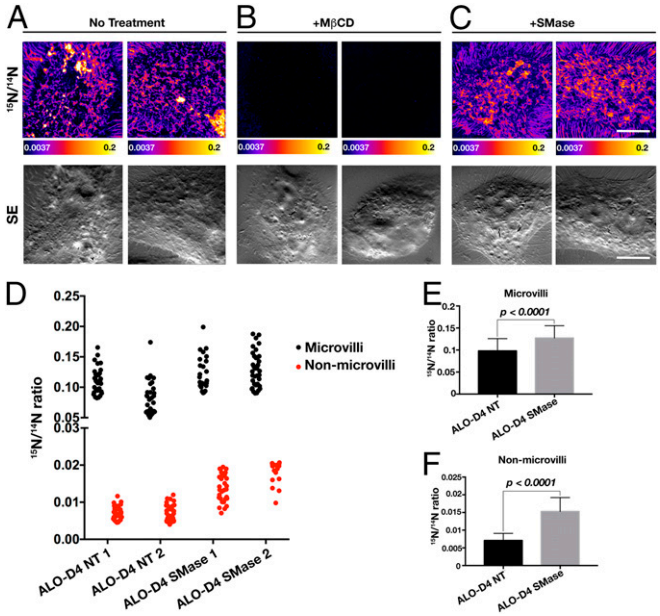

Fig. 3. NanoSIMS imaging of [^{15}N]ALO-D4 binding to the plasma membrane of CHO-KI cells that had been loaded with cholesterol. CHO-K1 cells were plated on silicon wafers and grown for 5 d. The cells were then loaded with cholesterol by incubating the cells for 2 d in medium containing 300 μM cholesterol (*Materials and Methods*). The cells were then washed and grown without supplemental cholesterol for 44 h. Next, the cells were plated on silicon wafers, grown overnight, and then given no treatment (*A*); treated with 10 mM methyl-β-cyclodextrin for 15 min at 37 °C (+MβCD) (*B*); or treated with 100 milliunits/mL of sphingomyelinase for 30 min at 37 °C (+SMase) (*C*). The cells were then washed and incubated with 20 μg/mL [^{15}N]ALO-D4 for 2 h at 4 °C. NanoSIMS images were generated based on secondary electrons (SEs) and on the ratio of $^{12}C^{15}N^-$ to $^{12}C^{14}N^-$ secondary ions ($^{15}N/^{14}N$). (Scale bar, 10 μm.) The color scale shows the range of $^{15}N/^{14}N$ ratios. (*D*) $^{15}N/^{14}N$ ratios in microvilli (black solid circles) and nonmicrovilli regions (red solid circles) (n = 30) of two nontreated (NT) and SMase-treated (SMase) cells. (*E* and *F*) Bar graphs of $^{15}N/^{14}N$ ratios in microvilli and nonmicrovilli regions on the plasma membrane of NT and SMase-treated cells. Data were analyzed with an unpaired Student's t test with Welch's correction.

NanoSIMS images (Fig. 1*C*). Using those images, we analyzed the $^{15}N/^{14}N$ ratio along straight lines that traversed microvilli; these line scans revealed that $^{15}N/^{14}N$ ratios were about fivefold higher in microvilli than in surrounding regions free of microvilli ("meadows") (Fig. 1*D*). The high-resolution NanoSIMS images had a lateral resolution of 70 nm (Fig. 1*F*) by the 16–84% definition (9). Microvilli on CHO-K1 cells on silicon wafers were also documented by scanning electron microscopy (Fig. 1 *E* and *F*).

To gauge the specificity of [^{15}N]ALO-D4 binding to cholesterol, we performed NanoSIMS imaging of cells in which cholesterol stores had been depleted with MβCD and cells in which the sphingomyelin-sequestered cholesterol pool had been released with SMase. In our first such experiments, we used CHO cells that had been cultured under standard conditions (i.e., no supplemental cholesterol) (Fig. 2). In the absence of MβCD or SMase, the $^{15}N/^{14}N$ images revealed preferential binding of [^{15}N]ALO-D4 to microvilli on the plasma membrane (Fig. 2*A*). Treatment of cells with MβCD virtually eliminated [^{15}N]ALO-D4 binding to cells (Fig. 2*B*). After SMase treatment of cells, the binding of [^{15}N]ALO-D4 increased (Fig. 2*C*). Further analyses revealed that SMase treatment resulted in an average sixfold increase in the $^{15}N/^{14}N$ ratio on microvilli but only an approximately twofold increase in adjacent meadows (Fig. 2 *D–F*). When $^{15}N/^{14}N$ ratios from entire cells were considered, they were 0.014 ± 0.003 in nontreated cells, 0.0037 ± 0.0002 in MβCD-treated cells (identical to the natural abundance of ^{15}N), and 0.057 ± 0.0096 in SMase-treated cells.

NanoSIMS imaging of [^{15}N]ALO-D4 binding was also performed on CHO-K1 cells that had been loaded with cholesterol (Fig. 3). As expected, the amount of [^{15}N]ALO-D4 binding to cells was higher in cholesterol-loaded cells ($^{15}N/^{14}N$ ratio of 0.033 ± 0.0025 vs. 0.014 ± 0.003 in cells grown without supplemental cholesterol). Again, [^{15}N]ALO-D4 bound preferentially to microvilli (Fig. 3*A*), and the binding of [^{15}N]ALO-D4 to cells was virtually eliminated by MβCD (Fig. 3*B*). Treatment of cholesterol-loaded cells with SMase resulted in increased [^{15}N]ALO-D4 binding ($^{15}N/^{14}N$ ratio of 0.042 ± 0.0018 vs. 0.033 ± 0.0025 in nontreated cells) (Fig. 3*C*). In the cholesterol-loaded cells, SMase treatment increased the $^{15}N/^{14}N$ ratio in microvilli but only by ∼30% (Fig. 3 *D–F*), whereas the $^{15}N/^{14}N$ ratio in meadows nearly doubled.

NanoSIMS imaging was sufficiently sensitive to visualize nonspecific binding of [^{15}N]ALO-D4 to the polylysine-coated silicon wafer substrate (Fig. S1). When we quantified ^{15}N enrichment in cell-free regions of the silicon wafer substrate (between microvilli at the edges of cells), we found a $^{15}N/^{14}N$ ratio of ∼0.006 (greater than ^{15}N's natural abundance), implying that there was nonspecific binding of [^{15}N]ALO-D4 to the polylysine-coated silicon wafer substrate. The $^{15}N/^{14}N$ ratio in the plasma membrane of cells on the

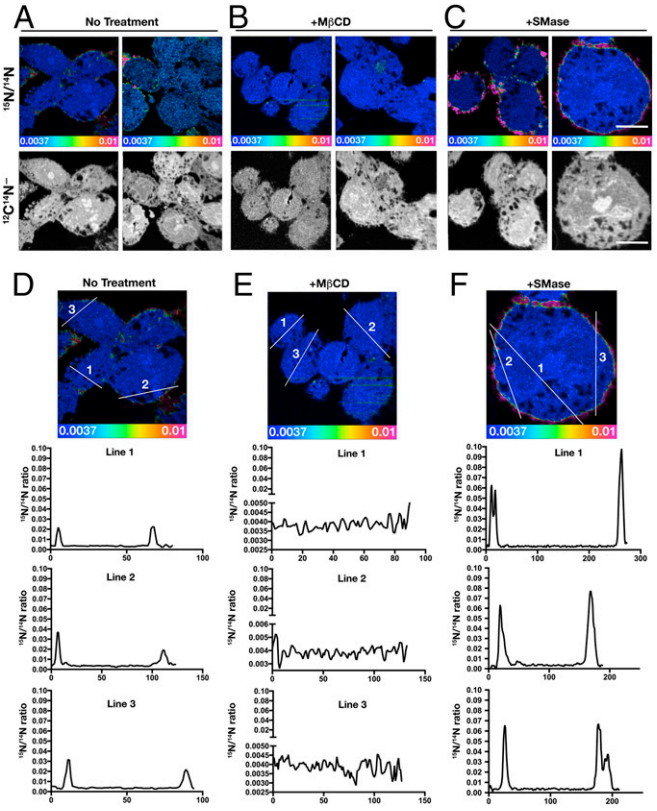

Fig. 4. NanoSIMS analysis of [^{15}N]ALO-D4 binding to CHO-K1 cells. CHO-K1 cells were plated on Thermanox plastic coverslips and grown for 5 d. The cells were then loaded with cholesterol as described in *Materials and Methods*. Coverslips received no treatment (*A*); treatment with 10 mM methyl-β-cyclodextrin for 15 min at 37 °C (+MβCD) (*B*); or treatment with 100 milliunits/mL of sphingomyelinase for 30 min at 37 °C (+SMase) (*C*). The cells were then washed and incubated with 20 μg/mL [^{15}N]ALO-D4 at 4 °C for 2 h. Next, the cells were fixed, dehydrated, resin embedded, and sectioned. NanoSIMS images were generated based on $^{12}C^{14}N^-$ secondary ions (to define cell morphology) and $^{15}N/^{14}N$ ratios {to visualize binding of [^{15}N]ALO-D4}. Peaks in $^{15}N/^{14}N$ ratios on the line graphs are centered above the plasma membrane. (Scale bar, 10 μm.) (*D–F*) Line graphs showing $^{15}N/^{14}N$ ratios across cells.

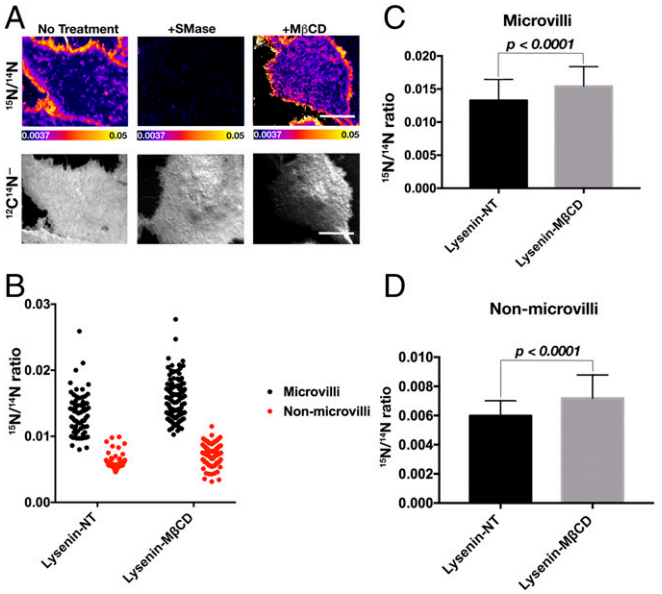

Fig. 5. NanoSIMS imaging of [^{15}N]lysenin binding to CHO-K1 cells. CHO-K1 cells were plated on silicon wafers. (*A*) The cells received either no treatment (NT); treatment with 100 milliunits/mL of sphingomyelinase for 30 min at 37 °C (+SMase); or treatment with 10 mM MβCD for 15 min (+MβCD) at 37 °C. The cells were then washed and incubated with 20 μg/mL [^{15}N]lysenin for 1 h at 4 °C. NanoSIMS images were generated based on $^{12}C^{14}N^-$ secondary ions (to define cell morphology) and on the $^{15}N/^{14}N$ ratio {to visualize [^{15}N]lysenin binding}. (Scale bar, 10 μm.) (*B*) $^{15}N/^{14}N$ ratios in microvilli (black solid circles) and nonmicrovilli regions (red solid circles) (n = 60) of nontreated and MβCD-treated cells. (*C* and *D*) Bar graphs depicting $^{15}N/^{14}N$ ratios in microvilli and in nonmicrovilli regions of NT cells and MβCD-treated cells. Data were analyzed with a Student's t test with Welch's correction and with a Mann–Whitney test. Both tests yielded the same level of statistical significance.

same silicon wafer was 0.033 ± 0.0025. In cells that had been treated with MβCD, the $^{15}N/^{14}N$ ratio in the plasma membrane fell to 0.0038 ± 0.0001 (very close to the natural abundance of ^{15}N), demonstrating that MβCD was effective in eliminating specific binding of [^{15}N]ALO-D4 to plasma membrane cholesterol. In contrast, the $^{15}N/^{14}N$ ratio of the cell-free substrate was 0.006 (Fig. S1). Thus, the low levels of nonspecific [^{15}N]ALO-D4 binding to the polylysine-coated silicon wafer substrate were not altered by MβCD.

In the NanoSIMS images shown in Figs. 1–3, which were acquired with cells plated on silicon wafers, our assumption was that [^{15}N]ALO-D4 binding was confined to the plasma membrane. To assess the validity of this assumption, we performed NanoSIMS analysis on sections of cells. The NanoSIMS images of sectioned cells (Fig. 4) revealed that the ^{15}N-enrichment was confined to the plasma membrane (Fig. 4 *A*–*C*). Again, [^{15}N]ALO-D4 binding to the plasma membrane was virtually eliminated by MβCD, whereas [^{15}N]ALO-D4 binding increased after SMase treatment (Fig. 4 *A*–*C*). Line diagrams revealed a high $^{15}N/^{14}N$ ratio over the plasma membrane, whereas the $^{15}N/^{14}N$ ratio inside the cells was identical to the natural value (0.0037) (Fig. 4 *D*–*F*).

An earlier NanoSIMS study found large patches of sphingolipids on the plasma membrane of 3T3 fibroblasts, whereas cholesterol was distributed evenly (5). However, because cholesterol and sphingomyelin are thought to interact loosely and transiently in the plasma membrane, we wanted to examine sphingomyelin distribution on the plasma membrane with lysenin (a sphingomyelin-binding protein). We prepared a ^{15}N-labeled lysenin, incubated it with CHO-K1 cells, and then used NanoSIMS imaging to assess the distribution of lysenin binding (Fig. 5). As judged by $^{15}N/^{14}N$ images, [^{15}N]lysenin appeared to bind preferentially to microvilli (Fig. 5*A*). Treatment of cells with SMase markedly reduced [^{15}N]lysenin binding (Fig. 5*B*). The $^{15}N/^{14}N$ ratio in the entire plasma membrane of SMase-treated cells was 0.0043 ± 0.0003 vs. 0.012 ± 0.0001 in nontreated cells. In MβCD-treated cells, the $^{15}N/^{14}N$ ratio was slightly higher (0.016 ± 0.0063) (Fig. 5*C*). Further analyses showed a higher $^{15}N/^{14}N$ ratio in microvilli of MβCD-treated cells (Fig. 5 *D*–*F*). The finding of increased lysenin binding to MβCD-treated cells contrasts with findings of an earlier study (10) and raises the possibility that depletion of plasma membrane cholesterol might increase accessibility of plasma membrane sphingomyelin to lysenin.

Confocal microscopy confirmed that ALO-D4 and lysenin bind preferentially to microvilli at the edges of cells (Fig. 6) but the colocalization of ALO-D4 and lysenin was not perfect (e.g., there were patches of lysenin binding that did not coincide with ALO-D4 binding). Confocal microscopy allowed us to detect large differences in ALO-D4 and lysenin binding (e.g., reduced ALO-D4 binding to MβCD-treated cells or reduced lysenin binding to SMase-treated cells) (Fig. 6). However, confocal imaging did not allow us to be confident about smaller changes, for example increased binding of ALO-D4 to SMase-treated cells (Fig. 6).

Discussion

We used NanoSIMS imaging to visualize and quantify the binding of ^{15}N-labeled cholesterol- and sphingomyelin-binding proteins to the plasma membrane of CHO cells. Earlier biochemical studies (2) thoroughly characterized ^{125}I-PFO* to fibroblasts and CHO cells but did not address whether the amount of PFO* binding is influenced by morphologic or topographic features of the plasma membrane. In this study, we chose to investigate the binding of PFO* and ALO-D4 to CHO cells because ultrastructural studies had shown that the surface of CHO cells is not flat and featureless but instead complex—with numerous microvilli projecting from the surface of the cells (11). One of our goals was to define (and quantify) the relationship between cell morphology and PFO* and ALO-D4 binding. NanoSIMS is ideal for this purpose because it provides high-resolution images—higher than those obtained by

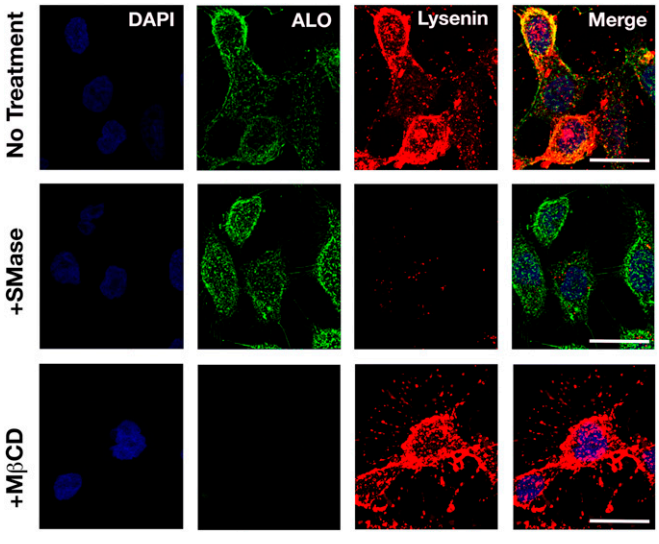

Fig. 6. Immunofluorescence microscopy to assess the binding of ALO-D4 and mCherry-lysenin to CHO-K1 cells. CHO-K1 cells were plated on glass coverslips and grown overnight before receiving one of three treatments: incubating cells in medium alone at 37 °C for 30 min (i.e., no treatment); incubating cells with medium containing 100 milliunits/mL of SMase at 37 °C for 30 min (+SMase); or incubating cells with medium containing 10 mM MβCD at 37 °C for 15 min (+MβCD). Binding of ALO-D4 and lysenin to the surface of cells was assessed by confocal microscopy as described in *SI Materials and Methods*. Cell nuclei were visualized with DAPI (blue). (Scale bar, 20 μm.)

confocal microscopy (12). Also, NanoSIMS offers the unique capability to correlate chemical information (e.g., specific secondary ions) to high-resolution morphology. In our study, we assessed binding of the lipid-binding proteins to cells by calculating the ratio of $^{12}C^{15}N^-$ ions (from ^{15}N-labeled proteins) to $^{12}C^{14}N^-$ ions (from lipids and proteins of the plasma membrane). Images of secondary electrons or $^{12}C^{14}N^-$ ions were used to define cell morphology. We found that the binding of PFO* and ALO-D4 to the plasma membrane was not uniform; instead, these proteins bind preferentially to microvilli. Lysenin, a sphingomyelin-binding protein, also bound preferentially to microvilli on cells.

Our NanoSIMS images showed markedly reduced [^{15}N]ALO-D4 binding to MβCD-treated cells and significantly increased [^{15}N]ALO-D4 binding to SMase-treated cells. These findings are entirely consistent with the biochemical findings by Das et al. (2). However, NanoSIMS analysis provided a more nuanced understanding of ALO-D4 binding to cells, showing that [^{15}N]ALO-D4 binds in a preferential fashion to microvilli. In addition, when CHO-K1 cells grown under standard conditions were treated with SMase, NanoSIMS analysis revealed an ∼10-fold increase in [^{15}N]ALO-D4 binding to microvilli. When the cells were loaded with cholesterol and subsequently treated with SMase, [^{15}N]ALO-D4 binding to microvilli increased by only about 30%. These results suggest that numbers of ALO-D4 binding sites on microvilli of cholesterol-loaded cells were close to maximal, such that release of "sphingomyelin-sequestered cholesterol" had a limited capacity to increase ALO-D4 binding.

The finding that accessible cholesterol is enriched in microvilli is potentially relevant to cholesterol transport. Microvilli vastly increase the surface area of the plasma membrane without necessitating a large increase in cell volume. In intestinal enterocytes, microvilli are essential for absorption of nutrients. However, microvilli exist in many other cell types and are likely relevant to nutrient transfer as well. For example, microvilli on parenchymal cells of the adrenal gland have been proposed to play a role in cholesterol transport (13). Along these lines, we suspect that the high levels of accessible cholesterol on microvilli of CHO cells (as judged by high levels of ALO-D4 binding), could facilitate transfer of cholesterol away from the plasma membrane.

Studies of model membranes have suggested that cholesterol can affect membrane curvature and in some cases may promote positive membrane curvature (14, 15). Thus, one possibility is that a large amount of cholesterol in plasma membrane microvilli is relevant to both membrane curvature and increased ALO-D4 binding. A second possibility (perhaps more likely and not mutually exclusive) is that the curvature of the plasma membrane (dictated by the actin cytoskeleton) causes cholesterol to be more exposed, thereby facilitating ALO-D4 binding. In highly curved membranes, such as those covering microvilli, it is possible that the polar regions of lipids at the surface of the exofacial leaflet are less densely packed than the acyl chains of plasma membrane phospholipids. Such a scenario might facilitate ALO-D4 binding. The NanoSIMS images in the current studies cannot distinguish between the two possibilities, but it is conceivable that future NanoSIMS experiments could be useful. In principle, it might be possible to load cultured cells with [^{18}O]cholesterol (5) and then use NanoSIMS imaging to quantify [^{15}N]ALO-D4 binding, relative to [^{18}O]cholesterol, in both microvilli and regions of the plasma membrane lacking microvilli. In preliminary studies, we attempted to visualize [^{18}O]cholesterol in the plasma membrane of [^{18}O]cholesterol-loaded cells, but we were not successful. We found abundant [^{18}O]cholesterol in cytosolic lipid droplets, but the amounts of [^{18}O]cholesterol in the plasma membrane were not sufficient to visualize microvilli at the edges of cells.

Our NanoSIMS images suggested that the distributions of ALO-D4 and lysenin binding sites on the plasma membrane were similar (but not identical) to preferential binding to microvilli. Earlier NanoSIMS images of 3T3 fibroblasts revealed distinct distributions for [^{18}O]cholesterol and [^{15}N]sphingolipids on the plasma membrane (5). One obvious explanation for the different results is that the two studies used different cell lines. Another is that the numbers of ^{18}O secondary ions in the 3T3 fibroblast studies may not have been sufficient to discern nonhomogeneities in cholesterol distribution. Also, the ^{18}O secondary ions in the 3T3 cell studies would likely reflect all cholesterol molecules in the plasma membrane, whereas the ^{15}N ions in our studies would reflect only the accessible cholesterol pool. Again, it is conceivable that one could resolve the distribution of accessible cholesterol from the total cholesterol pool by examining [^{15}N]ALO-D4 binding to cells that had been loaded with ^{13}C- or ^{18}O-labeled cholesterol, but those sorts of studies could prove to be challenging. Aside from needing to enrich cells with sufficient amounts of labeled cholesterol for imaging, one would need to be confident that the secondary ions released from cells actually originate from labeled cholesterol on the plasma membrane. Recent time-of-flight secondary ion mass spectrometry (TOF-SIMS) studies of cholesterol in fixed mouse brain sections suggested that cholesterol can migrate from deeper portions of the section to the surface of the section, and that this apparent migration occurs under experimental conditions similar to those used in NanoSIMS imaging (16).

ACKNOWLEDGMENTS. We thank Dr. Arun Radhakrishnan for PFO* and ALO-D4 vectors and for scientific discussions, Frederick Maxfield for helpful discussions, and the NanoSIMS facilities at Caltech and the University of Western Australia for technical guidance. We acknowledge support from Leducq Foundation Transatlantic Network Grant 12CVD04 (to S.G.Y.); National Institutes of Health Grants P01 HL090553 (to S.G.Y.), R01 HL087228 (to S.G.Y.), and HL125335 (to S.G.Y.); the Ruth L. Kirschstein National Research Service Award F32 HL132471 (to C.H.); the Australian Microscopy and Microanalysis Research Facility; the Science and Industry Endowment Fund; and the State Government of Western Australia.

1. Das A, Goldstein JL, Anderson DD, Brown MS, Radhakrishnan A (2013) Use of mutant 125I-perfringolysin O to probe transport and organization of cholesterol in membranes of animal cells. *Proc Natl Acad Sci USA* 110(26):10580–10585.
2. Das A, Brown MS, Anderson DD, Goldstein JL, Radhakrishnan A (2014) Three pools of plasma membrane cholesterol and their relation to cholesterol homeostasis. *eLife* 3:02882.
3. Brown DA, Rose JK (1992) Sorting of GPI-anchored proteins to glycolipid-enriched membrane subdomains during transport to the apical cell surface. *Cell* 68(3):533–544.
4. Owen DM, Magenau A, Williamson D, Gaus K (2012) The lipid raft hypothesis revisited: New insights on raft composition and function from super-resolution fluorescence microscopy. *BioEssays* 34(9):739–747.
5. Frisz JF, et al. (2013) Sphingolipid domains in the plasma membranes of fibroblasts are not enriched with cholesterol. *J Biol Chem* 288(23):16855–16861.
6. Jiang H, et al. (2014) High-resolution imaging of dietary lipids in cells and tissues by NanoSIMS analysis. *J Lipid Res* 55(10):2156–2166.
7. Gay A, Rye D, Radhakrishnan A (2015) Switch-like responses of two cholesterol sensors do not require protein oligomerization in membranes. *Biophys J* 108(6):1459–1469.
8. Hotze EM, et al. (2002) Monomer-monomer interactions drive the prepore to pore conversion of a beta-barrel-forming cholesterol-dependent cytolysin. *J Biol Chem* 277(13):11597–11605.
9. Lechene C, et al. (2006) High-resolution quantitative imaging of mammalian and bacterial cells using stable isotope mass spectrometry. *J Biol* 5(6):20.
10. Mizuno H, et al. (2011) Fluorescent probes for superresolution imaging of lipid domains on the plasma membrane. *Chem Sci* 2:1548–1553.
11. Carpentier JL, Paccaud JP, Gorden P, Rutter WJ, Orci L (1992) Insulin-induced surface redistribution regulates internalization of the insulin receptor and requires its autophosphorylation. *Proc Natl Acad Sci USA* 89(1):162–166.
12. Saka SK, et al. (2014) Correlated optical and isotopic nanoscopy. *Nat Commun* 5: 3664.
13. Reaven E, Spicher M, Azhar S (1989) Microvillar channels: A unique plasma membrane compartment for concentrating lipoproteins on the surface of rat adrenal cortical cells. *J Lipid Res* 30(10):1551–1560.
14. Chen Z, Rand RP (1997) The influence of cholesterol on phospholipid membrane curvature and bending elasticity. *Biophys J* 73(1):267–276.
15. Sodt AJ, Venable RM, Lyman E, Pastor RW (2016) Nonadditive compositional curvature energetics of lipid bilayers. *Phys Rev Lett* 117(13):138104.
16. Sjovall P, Johansson B, Lausmaa J (2006) Localization of lipids in freeze-dried mouse brain sections by imaging TOF-SIMS. *Appl Surf Sci* 252:6966–6974.